Drivers and mechanisms contributing to excess warming in Europe during recent decades

Dong, B. ORCID: https://orcid.org/0000-0003-0809-7911 and Sutton, R. T. ORCID: https://orcid.org/0000-0001-8345-8583
(2025) Drivers and mechanisms contributing to excess warming in Europe during recent decades. npj Climate and Atmospheric Science, 8. 41. ISSN 2397-3722 doi: 10.1038/s41612-025-00930-3 Available at https://centaur.reading.ac.uk/120676/

npj | climate and atmospheric science

Article

Published in partnership with CECCR at King Abdulaziz University

https://doi.org/10.1038/s41612-025-00930-3

Drivers and mechanisms contributing to excess warming in Europe during recent decades

Buwen Dong ✉ & Rowan T. Sutton

Over the period 1979-2022, European surface air temperatures warmed around three times as fast as the global mean temperatures in both winter and summer. Here we define "excess" European warming as the difference between the rate of European regional warming and the rate of global warming and investigate the causes. Using a simple observation-based method, we estimate that around 40% ± 39% (in winter) and 29% ± 10% (in summer) of excess European warming is "dynamical" - attributable to changes in atmospheric circulation. We show that the rate of European warming simulated in CMIP6 models compares well with the observations, but only because these models warm too fast in the global mean; excess European warming is underestimated, particularly in winter. The CMIP6 models simulate well the magnitude of the thermodynamic component of excess European warming since 1979 in both winter and summer, they suggest only a weak dynamical contribution in the multi-model mean. The models suggest greenhouse gas-induced warming made the largest contribution to excess thermodynamic warming in winter, whereas changes in anthropogenic aerosols made the largest contribution in summer. They also imply a substantially reduced future rate of excess European warming in summer. However, the failure of current models to simulate observed circulation trends (either as a forced response or as a combination of forced response and internal variability) also implies large uncertainty in future rates of European warming.

Trends in surface air temperature (SAT) during recent decades exhibit a nonuniform pattern with amplified warming over Europe in both winter and summer (Fig. 1a, b). Indeed, Europe has been the fastest-warming continent on the Earth, warming more than twice as fast as the global mean over recent decades (Fig. 1e, f), consistent with previous studies[1–3]. The rapid warming in summer is associated with increases in intense and longer-lasting extreme heatwaves, sometimes coupled with droughts, and has led to Europe being identified as a heatwave hotspot[4–13]. Meanwhile, the warming in winter is associated extreme rainfall events, increased runoff, and risk of flooding, related to changes in atmospheric circulation and precipitation characteristics[7,14–16]. In view of these changes in climate extremes and their impacts, further understanding European excess warming, including whether it may continue in the future, is an important challenge. For the purposes of this study, we define excess European warming as the difference between the rate of European regional warming and the rate of global warming.

Regional warming on decadal-multidecadal scales is influenced by global and regional drivers, such as radiative forcings from anthropogenic greenhouse gases (GHGs)[1,17,18], anthropogenic aerosol emissions (AER)[18–21], changes in solar activity and large-scale volcanic eruptions[22], and by modes of internal climate variability, such as the North Atlantic Oscillation (NAO)[23–27], and Atlantic Multidecadal Variability (AMV)[28–30]. Previous studies have demonstrated the important influence of atmospheric circulation on warming over Europe in both winter and summer[1,23,25–27,31] and for understanding trends in hot extremes in Europe[8,11,32,33]. However, it remains unclear whether the relevant changes in atmospheric circulation are the result of natural climate variability or are responses to natural or anthropogenic external forcings[11,34]. Furthermore, past studies concluded that previous generations of CMIP3 and CMIP5 models[35] tended to underestimate the observed warming trend in summer over Western Europe, linked in part to a failure to simulate observed atmospheric circulation changes over the Atlantic sector[1,36,37]. Given the outstanding knowledge gaps, there is a clear need to investigate further the drivers and underlying mechanisms that may be responsible for the observed excess warming in Europe, and the extent to which these mechanisms may be accurately simulated in the latest models.

In this study, we first analyze observational and reanalysis data sets to quantify regional warming trends over Europe in boreal winter and summer

National Centre for Atmospheric Science, Department of Meteorology, University of Reading, Reading, United Kingdom. ✉e-mail: b.dong@reading.ac.uk

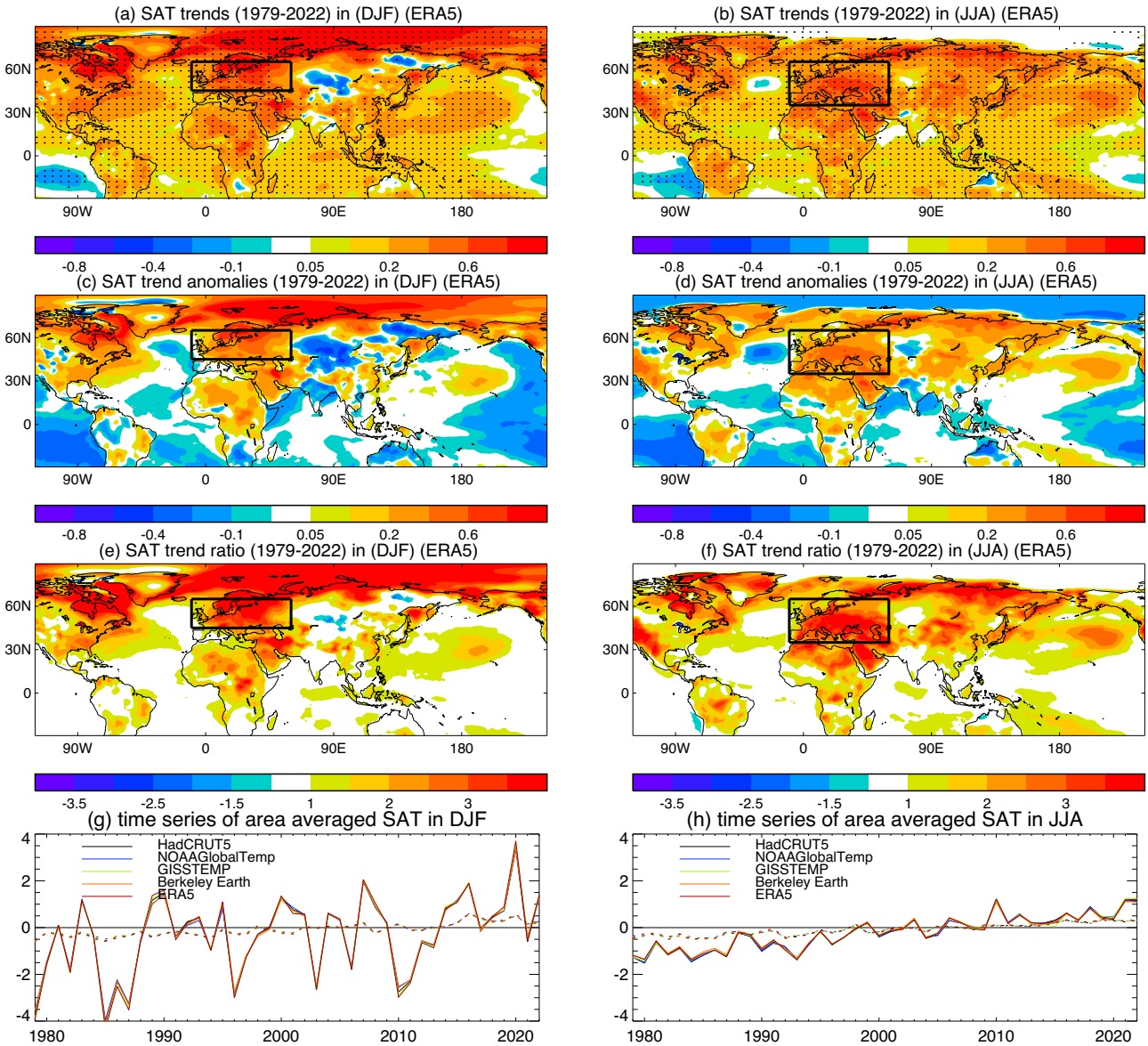

Fig. 1 | Linear trends of surface air temperature (SAT) in winter (December, January, February) and summer (June, July, August) during 1979-2022. a, **b** SAT trends (°C decade^{-1}), **c**, **d** trends at each grid point minus the global mean trend, **e**, **f** trend ratios at each grid point relative to the global mean trend. **a**, **c**, **e** DJF and **b**, **d**, **f** JJA during 1979-2022 based on ERA5 reanalysis. Trends that are significantly different from 0 at the 10% level using the Mann-Kendall test are dotted in panels (**a**, **b**). **g**, **h** Time series of area-averaged SAT anomalies over Europe (full lines) in DJF over the region (45°N-65°N, 10°W-60°E, black box in **a**, **c**, **e**), in JJA over the region (35°N-65°N, 10°W-60°E, black box in **b**, **d**, **f**), and corresponding global averaged anomalies (dotted lines) during 1979-2022 based on four observational data sets and ERA5 reanalysis.

- including the excess regional warming relative to the global mean - focusing on the period 1979-2022. Next, we investigate the contribution of atmospheric circulation to excess European warming using a simple regression-based method. Lastly, we use multimodel simulations from the coupled model intercomparison project phase 6 (CMIP6)[38] and detection and attribution model intercomparison project (DAMIP) single forcing experiments[39] to investigate the drivers and physical processes that contribute to excess European warming (see Methods).

Results

Excess warming over Europe in observations and reanalyses

The spatial patterns of surface air temperature (SAT) trends based on ERA5 reanalysis during last four decades show relatively large warming trends over Europe and weak trends over the North Atlantic subpolar gyre in both winter and summer (Fig. 1a-b) with excess European warming relative to global means (Fig. 1c-d). Other regions of excess warming are found over Eastern North America and the Middle-East in winter and western North America and the Middle-East in summer. However, we note that, when normalised by interannual variability, Europe stands out from other northern midlatitude continental regions in showing high signal-to-noise warming (Supplementary Fig. S1). The linear trends of SAT over Europe are around three times as high as the trends in global mean SAT (Fig. 1e-f). Four observational datasets and the ERA5 reanalysis show very consistent interannual variability of area-averaged SAT over Europe and the globe, and also show robust linear trends (Fig. 1g-h). The multi-dataset mean trends of area-averaged SAT over Europe during 1979-2022 are 0.52 ± 0.15 and 0.48 ± 0.03 °C decade^{-1} (Table 1) corresponding to total changes of 2.29 ± 0.66 and 2.10 ± 0.13 °C) in winter and summer respectively (80% confidence interval, see Methods), and these trends are 3.1 ± 1.0 and 2.8 ± 0.2 times the corresponding global mean trends (0.17 ± 0.02 and

Table 1 | Linear trends of SAT indices and the confidence interval (CI) in observations/reanalyses and CMIP6 (DAMIP) simulations

		Obs (79-22)	Obs (79-20)	CMIP6	GHG	AER	NAT	SUM
DJF	Europe	0.52 ± 0.15	0.54 ± 0.17	0.45 ± 0.10	0.32 ± 0.08	0.02 ± 0.08	0.06 ± 0.09	0.40 ± 0.17
	Global	0.17 ± 0.02	0.18 ± 0.02	0.25 ± 0.04	0.24 ± 0.03	-0.01 ± 0.02	0.02 ± 0.01	0.25 ± 0.05
	Eu-GL	0.35 ± 0.15	0.37 ± 0.16	0.20 ± 0.09	0.08 ± 0.08	0.03 ± 0.06	0.04 ± 0.09	0.15 ± 0.16
JJA	Europe	0.48 ± 0.03	0.45 ± 0.04	0.51 ± 0.07	0.26 ± 0.05	0.16 ± 0.05	0.04 ± 0.02	0.46 ± 0.10
	Global	0.17 ± 0.01	0.17 ± 0.01	0.25 ± 0.03	0.21 ± 0.02	0.01 ± 0.02	0.02 ± 0.01	0.24 ± 0.05
	Eu-GL	0.31 ± 0.03	0.28 ± 0.03	0.26 ± 0.05	0.05 ± 0.04	0.15 ± 0.04	0.02 ± 0.02	0.22 ± 0.07

Multi-dataset mean linear trends of SAT (°C decade^{-1}) based on four observations and ERA5 reanalysis during 1979-2022 and 1979-2020, and CMIP6 (DAMIP) multi-model mean values during 1979-2020 over Europe, Global, and their differences (Eu-GL, excess European warming) and uncertainty. SUM is the sum of model responses to GHG, AER, and NAT forcings. See Methods for details. For observations, the confidence interval is 80%, whereas for the model estimates a 95% range is shown. See Methods for details.

0.17 ± 0.01 °C decade^{-1}, corresponding to total changes of 0.76 ± 0.08 and 0.75 ± 0.04 °C). The SAT trends over Europe are also 2.0 ± 0.6 and 1.8 ± 0.2 times the corresponding global land mean trends and 1.8 ± 0.7 and 1.4 ± 0.1 times the corresponding zonal mean trends in winter and summer, respectively.

Estimating the contribution of atmospheric circulation to excess European warming

Associated with the excess European warming in winter, atmospheric circulation trends based on ERA5 show a spatial pattern over the North Atlantic sector which projects onto a positive NAO pattern in SLP, accompanied by a strengthening and eastward extension of the North Atlantic jet (Fig. 2a-c). The circulation trends based on the JRA55 reanalysis show very similar features (Supplementary Fig. S2). To quantify the contribution of atmospheric circulation trends to regional warming, we employ a simple regression-based method (see Methods). Specifically, we use the relationship between atmospheric circulation and SAT on interannual timescales to estimate the contribution from atmospheric circulation to the multidecadal warming trend. This approach is reasonable because the dominant patterns of atmospheric circulation show similar features on the different timescales, especially over Europe. A possible limitation of our method is that it considers only a single pattern of atmospheric circulation. However, we show in the Methods section that our approach nevertheless accounts for a larger component of the trend in European warming, in both winter and summer, than the sum of the contributions from the leading empirical orthogonal function (EOF) modes of atmospheric circulation. These findings suggest that the circulation indices we use are an efficient way to identify the dynamical contribution to trends in European temperatures.

Figure 2d-f show regression patterns for detrended winter SAT, 500 hPa zonal wind and SLP onto a detrended index of European SAT, thus highlighting interannual relationships. The patterns indicate that interannual warming over Europe is associated with a positive NAO phase and enhanced westerlies over the North Atlantic. The correlation coefficient between detrended NAO timeseries and SAT index time series over Europe is 0.74, which is statistically significant at the 5% level based on a two-tailed Student's t-test. As the circulation pattern associated with interannual variability shows considerable similarities over the North Atlantic-European sector to that associated with the multi-decadal trend (Fig. 2b-c), we use a NAO index to estimate the contribution of atmospheric circulation change to excess warming over Europe (see Methods). This estimated contribution is shown in Fig. 2g, with the residual warming shown in Fig. 2h. The positive NAO phase is associated with a northward shift in the North Atlantic jet stream, increased mid-latitude westerly winds in the northern part of the North Atlantic Ocean, hence causing warmer conditions than normal in western and Northern Europe[23,25] (Fig. 2d, e, f). For the European area average, the results suggest that *40% ± 39% of the excess warming (26% ± 24% of the total warming) in winter is explained by atmospheric circulation* (Fig. 2i, Table 2). To test robustness of this result to an alternative choice for the circulation index, we repeated the analysis using an index of zonal wind at 500 hPa, averaged over the North Atlantic jet exit region (45°N-60°N, 50°W-20°E). The results show that 37% ± 41% of the excess warming (24% ± 25% of the total warming) is explained by atmospheric circulation (Supplementary Fig. S3) based on the ERA5 reanalysis, with similar results using JRA55. These numbers are consistent with those obtained using the NAO index (Fig. 2g, h, i, Supplementary Fig. S3a, b, c).

Associated with excess warming trends over Europe in summer (Fig. 3a), atmospheric circulation trends based on ERA5 show an anomalous low over the North Atlantic[40], accompanied by a southward displacement of the North Atlantic jet, and an anomalous high over Europe, accompanied by a dipole structure of zonal wind trends over the European sector with a weakening of Mediterranean jet and increased westerlies to the north (Fig. 3b-c). Regression patterns of detrended circulation interannual variability onto a detrended SAT index over Europe show that warm summers are associated with an anomalous high over Europe, associated with a dipole pattern in zonal winds (Fig. 3d-f). This pattern of circulation anomalies over Europe is similar to that associated with the multi-decadal warming trend, although the pattern of anomalies over the North Atlantic is quite different. Focussing on Europe, we define a summer circulation index as the area averaged geopotential height over Europe (The trend in zonally averaged geopotential height over the same latitude band is first removed - see Methods). The correlation between detrended height time series and SAT index time series over Europe is 0.78, which is statistically significant at the 5% level based on a two-tailed Student's t-test. Following the same procedure as for winter, we use this index to quantify the contribution of atmospheric circulation change to excess summer warming over Europe. This estimated contribution is shown in Fig. 3g, with the residual warming shown in Fig. 3h. For the European area average, the results suggest that *29% ± 10% of the excess warming (19% ± 6% of the total warming) in summer is explained by atmospheric circulation* (Fig. 3i, Table 2). The circulation trends and the contribution of atmospheric circulation change to excess summer warming over Europe based on the JRA55 reanalysis show very similar features (Supplementary Fig. S4).

To test the robustness of this result to an alternative choice for the circulation index, we repeated the analysis using an index of zonal wind at 500 hPa, averaged over the Mediterranean (35°N-50°N, 0°-50°E) in summer. The results suggest that that 23% ± 4% of the excess warming (15% ± 2% of the total warming) is explained by atmospheric circulation (Supplementary Fig. S5) based on ERA5 with similar results in JRA55. These results suggest that the geopotential height index is a better choice in summer as it can account for a larger proportion of the excess and total European SAT trend.

Attribution of the observed warming trends

To investigate drivers of the observed excess warming over Europe we analyse multi-model simulations from the Coupled Model Intercomparison Project Phase 6 (CMIP6)[38], including both historical extended all forcing simulations (ALL) and single forcing simulations from the Detection and Attribution Model Intercomparison Project (DAMIP)[39] for the period 1979-2020 (see Methods, Supplementary Table S1). Similar to features seen

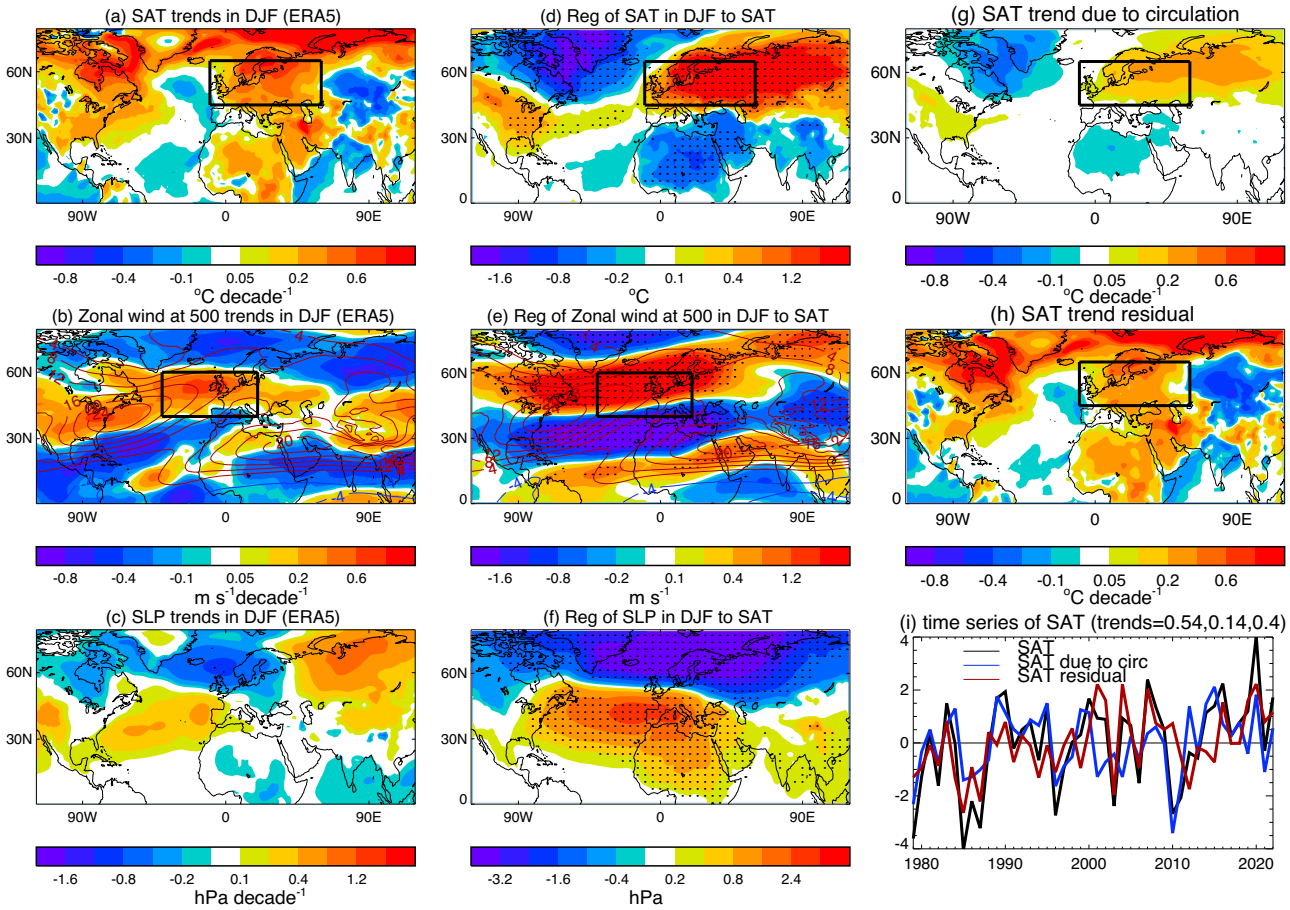

Fig. 2 | Linear trends of SAT, atmospheric circulation, regression patterns and circulation induced SAT trends in DJF based on ERA5 reanalysis during 1979-2022. a–c Linear trends of SAT (°C decade^{-1}), zonal wind (m s^{-1} decade^{-1}), and SLP (hPa decade^{-1}). **d–f** Regression patterns of SAT (°C), zonal wind (m s^{-1}) at 500 hPa, and SLP (hPa) in DJF to the normalized time series of European SAT index which is defined as the area averaged SAT over the region (45°N-65°N, 10°W-60°E, black box in **a**, **d**, **g**, **h**) in DJF with detrended data. **g**, **h** Linear trends of SAT due to circulation changes (°C decade^{-1}) and SAT residual trend (°C decade^{-1}). **i** Time series of SAT anomalies (black), relative contributions due to circulation changes (blue) and residuals (red) over Europe and linear trends (°C decade^{-1}; numbers in top right). The circulation index used for decomposition of SAT trends is the NAO index (see Methods). The global mean is removed in panels (**a**–**h**) and the removal of global mean has a very little impact on panels (**b**–**g**). Note that nonlinear color bar is used in all spatial patterns. The black box in (**b**) and (**e**) is used to define a zonal jet index over the North Atlantic jet exit region to test the sensitivity of the SAT trend decomposition to an alternative choice for the circulation index and results are shown in Supplementary Information Figure S3.

Table 2 | Linear trends of SAT, SAT trend due to circulation, SAT residual trend, and the confidence interval (CI)

		Europe (Total)	Europe (Circ)	Europe (Residual)	Global	Eu-GL	Eu/GL	Circ/Eu	Circ/(Eu-GL)
DJF	ERA5 (79-22)	0.54 ± 0.16	0.14 ± 0.12	0.40 ± 0.11	0.19 ± 0.02	0.35 ± 0.16	2.8 ± 0.9	26% ± 24%	40% ± 39%
	ERA5 (79-20)	0.56 ± 0.18	0.17 ± 0.13	0.39 ± 0.12	0.19 ± 0.02	0.37 ± 0.17	2.9 ± 1.0	30% ± 25%	46% ± 41%
	CMIP6	0.45 ± 0.10	0.01 ± 0.02	0.44 ± 0.01	0.25 ± 0.04	0.20 ± 0.09	1.8 ± 0.5	2% ± 4%	5% ± 10%
JJA	ERA5 (79-22)	0.48 ± 0.03	0.09 ± 0.03	0.39 ± 0.02	0.17 ± 0.01	0.31 ± 0.03	2.8 ± 0.2	19% ± 6%	29% ± 10%
	ERA5 (79-20)	0.45 ± 0.04	0.08 ± 0.03	0.37 ± 0.02	0.16 ± 0.01	0.29 ± 0.04	2.8 ± 0.3	18% ± 7%	28% ± 11%
	CMIP6	0.51 ± 0.07	-0.01 ± 0.01	0.52 ± 0.06	0.25 ± 0.03	0.26 ± 0.05	2.0 ± 0.4	-2% ± 2%	-4% ± 4%

Linear SAT trends (°C decade^{-1}) in ERA5 reanalysis during 1979-2022 and 1979-2020, CMIP6 multi-model mean trend during 1979-2020 over Europe (Total), and relative contributions of changes in circulations to the trend over Europe (Circ), residual trend over Europe (Residual), differences in trend between Europe and global (Eu-GL, excess European warming), percentage contributions of circulation induced SAT change to SAT trend over Europe (Circ/Eu) and to excess European warming (Circ/(Eu-GL). For observations, the confidence interval is 80%, whereas for the model estimates a 95% range is shown. See Methods for details.

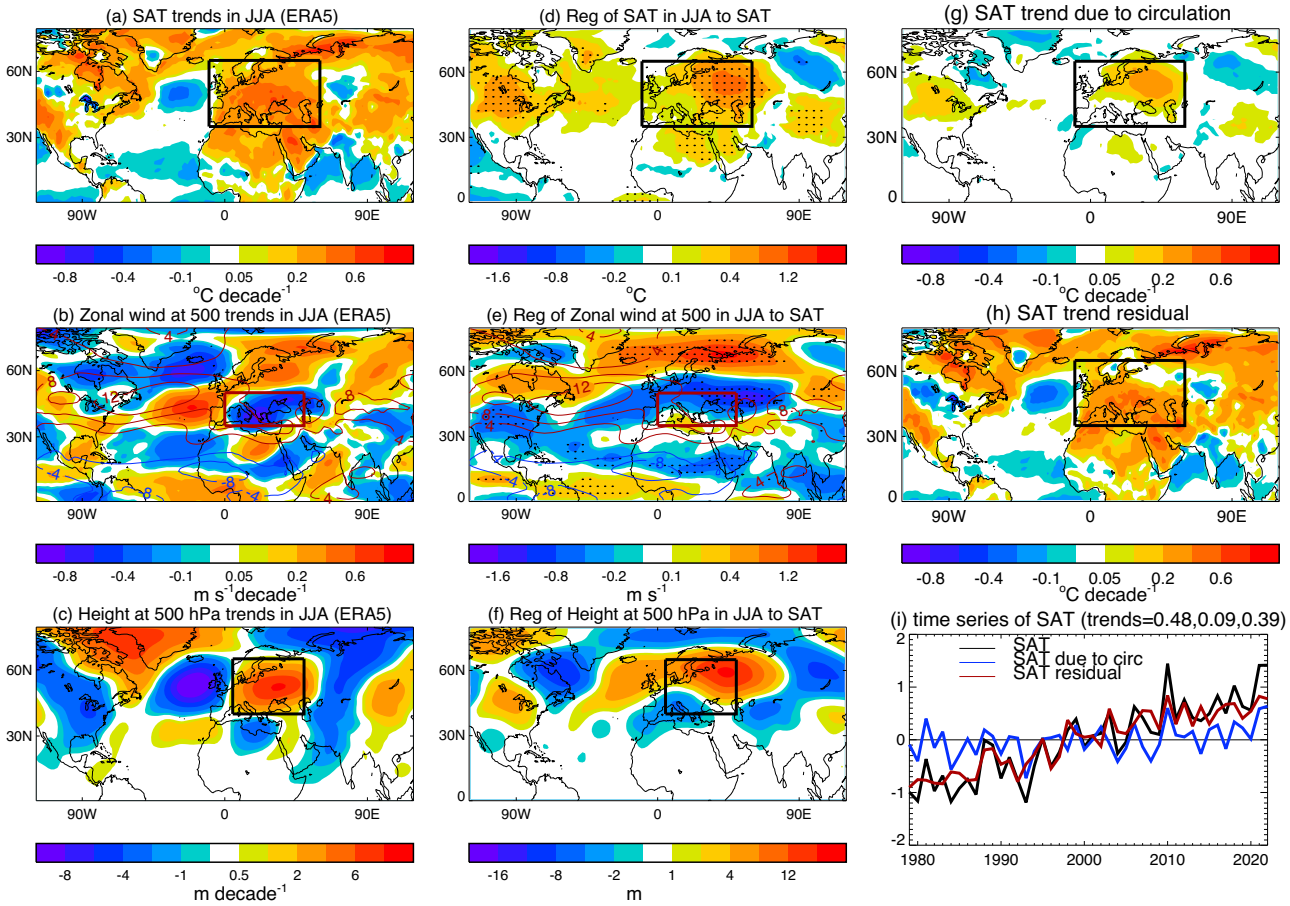

Fig. 3 | Linear trends of SAT, atmospheric circulation, regression patterns and circulation induced SAT trends in JJA based on ERA5 reanalysis during 1979-2022. a–c Linear trends of SAT (°C decade^{-1}), zonal wind (m s^{-1} decade^{-1}) and geopotential height (m decade^{-1}) at 500 hPa. **d–f** Regression patterns of SAT (°C), zonal wind (m s^{-1}) and geopotential height (m) at 500 hPa in JJA to the normalized time series of the European SAT index which is defined as area averaged SAT over the region (35°N-65°N, 10°W-60°E, black box in **a**, **d**, **g**, **h**) in JJA with detrended data. **g**, **h** SAT trends due to circulation changes (°C decade^{-1}) and SAT residual trend (°C decade^{-1}). **i** Time series of SAT anomalies over Europe and linear trends (°C decade^{-1}; numbers in top right). The circulation index used for decomposition of SAT trends is the height index (see Methods). The global mean is removed in panels (**a**, **b**, **d**, **e**, **g**, **h**) and the removal of global mean has a very little impact. Zonal mean is removed in panels (**c**) and (**f**). Note that nonlinear color bar is used in all spatial patterns. The red box in (**b**) and (**e**) is used to define a zonal jet index over the Mediterranean to test the sensitivity of SAT trend decomposition to an alternative choice for the circulation index and results are shown in Supplementary Information Figure S5.

in observations (Fig. 1a-b), Multi-model mean (MMM) responses to ALL forcing changes show large warming trends over the continents in the northern hemisphere in both winter and summer (Fig. 4a, b, Supplementary Fig. S6a, b). However, the model simulated warming over the continents is more uniform than is seen in observations. As a result, the ratio of European warming to global mean warming in the ALL simulations gives MMM values of 1.8 (with a range of 0.8-2.9) in winter and 2.1 (with a range of 1.7-2.8) in summer, which are about 40% and 25% lower than the observed values (Fig. 4i, j, Supplementary Fig. S8).

To identify the contribution of greenhouse gas (GHG), anthropogenic aerosols (AER) and natural (NAT) forcings to the excess warming over Europe, we use DAMIP single forcing experiments[39]. Note that anthropogenic aerosol emissions over Europe and North America peak around 1970s and decline after 1970s[41]. MMM results shows enhanced warming over mid-high northern latitudes in winter and a more uniform warming over land in summer in response to GHG forcing (Fig. 4b, f, Supplementary Fig. S6b, f). GHG forcing makes the largest contribution to absolute winter warming in Europe simply because GHG forcing contributes most to warming almost everywhere, but it doesn't follow that GHG should necessarily make the largest contribution (relative to other forcings) to the *excess* warming in Europe, since these contributions depend on the response patterns as well as their magnitudes. By contrast AER simulations show spatially inhomogeneous trends of SAT in summer, characterized by enhanced warming over mid-high latitude Eurasia and reduced warming over tropical Africa, and South and East Asia (Fig. 4g, Supplementary Fig. S6g). These results strongly suggest that the decline in AER forcing has been an important driver of the observed excess warming over Europe in summer over recent decades, consistent with other recent studies[12,18–21]. AER decline-induced warming trends in winter are weak over the Eurasian continent (Fig. 4c, Supplementary Fig. S6c). NAT forcing-induced SAT trends are generally weak and not consistent among different models in both winter and summer (Fig. 4d, h, Supplementary Fig. S6d, h).

To illustrate how unusual is the excess warming over Europe in response to ALL forcing in comparison with the warming trend seen in individual ensemble members, we calculated the multi-ensemble mean (MEM) spatial patterns of excess warming using all ensemble members of all models, corresponding inter-ensemble standard deviations in winter and summer and their ratios (Supplementary Fig. S7). The MEM patterns and magnitudes of excess warming in both seasons are very close to those in the multi-model mean (Supplementary Fig. S6a, b). The standard deviation of excess warming shows large inter-ensemble variability in the Arctic and in high latitudes over the Eurasian continent, including Europe in winter. As a result, the signal- to-noise ratio is lower over Europe. In contrast, the

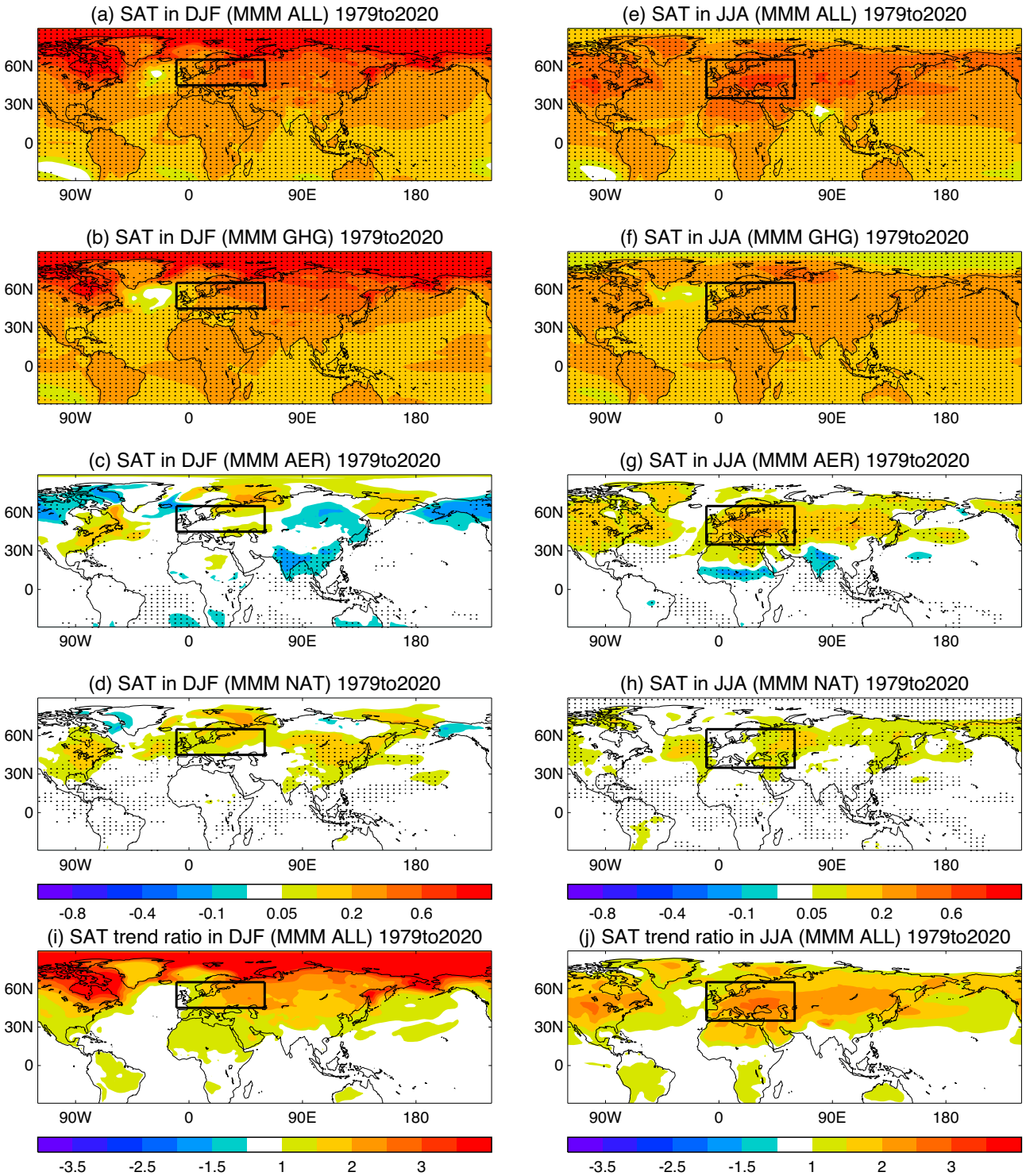

Fig. 4 | The multimodel mean (MMM) linear trends of SAT in winter (December, January, February) and summer (June, July, August) during 1979-2020 in CMIP6 historical extended (DAMIP) simulations. a–d SAT trends (°C decade^{-1}) in response to different forcings (ALL, GHG, AER, NAT) in DJF and **e–h** in JJA. Dots indicate regions where 80% of models have the same sign of trend. Note that nonlinear color bar is used in spatial patterns (**a–h**). **i, j** Local SAT trend ratio relative to global mean trend in DJF and JJA. The black box outlines the region that is used to define SAT index over Europe. The details for analyses of model simulations are in Methods.

standard deviation of excess warming in summer shows a weak and more uniform inter-ensemble variability over the Eurasian continent, leading to large signal-to-noise ratio, including over Europe, North Africa, and mid-latitudes over Asia in summer. These contrasting features of signal-to-noise ratio between winter and summer are consistent with the large intra-ensemble spread of the European excess warming in winter and weak spread in summer. Understanding both the model spread and the ensemble spread of responses is important, but beyond the scope of this study.

Quantitative comparisons between the SAT trends over Europe for multi-dataset mean in observations and MMM responses to different forcings are shown in Fig. 5 and in Table 1. Those for each observational dataset and for individual models, and individual ensemble members are shown in

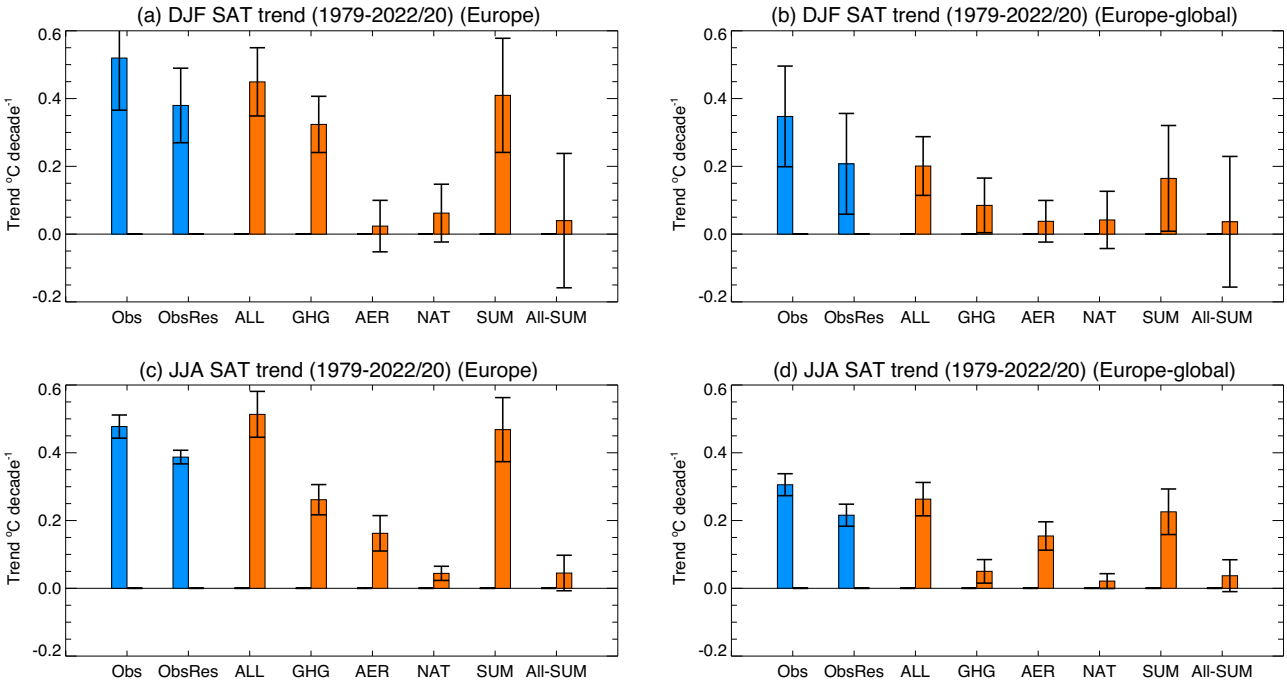

Fig. 5 | Linear trends of SAT indices and the confidence interval (CI) in winter (December, January, February) and summer (June, July, August) in observations/reanalyses and CMIP6 historical extended (DAMIP) simulations. a, **c** SAT (°C decade^{-1}) over Europe and **b**, **d** SAT trend difference between Europe and global mean in observations (blue bar) during 1979-2022 and model simulations (red bar) during 1979-2020 based on CMIP6/DAMIP model simulations in response to different forcings. **a**, **b** for DJF and **c**, **d** for JJA. ObsRes is the SAT residual trend with the circulation induced trend based on ERA5 reanalysis removed from the total SAT trend (see methods). SUM is the sum of model responses to GHG, AER, and NAT forcings. All-SUM is the difference between the response in ALL forcing and SUM. For observations the confidence interval shown is 80%, whereas for the model estimates a 95% range is shown. See Methods for details.

Supplementary Fig. S9 and Fig. S10. The MMM surface warming in winter over Europe in response to ALL forcings during 1979-2020 exhibits a trend of 0.45 ± 0.10 °C decade^{-1} (see Methods), which is slightly weaker (by about 13%) than the mean value based on the four observations and ERA5 reanalysis (0.52 ± 0.15 °C decade^{-1}) during 1979-2022. However, the MMM global warming is about 47% stronger than that based on observations (0.25 vs 0.17 °C decade^{-1}). This is consistent with higher climate sensitivity in CMIP6 models by comparison with CMIP5 models[42–44]. As a result, *the excess warming relative to global mean observed on Europe is severely underestimated (by about 43%) in the MMM*. Responses to different forcings show that the absolute and excess winter warming over Europe in the models is predominantly due to GHG forcings, with AER and NAT forcings making weak contributions (Fig. 5, Table 1).

In summer, the MMM simulated warming trend of 0.51 ± 0.07 °C decade^{-1} in response to ALL forcing changes is slightly stronger (by about 6%) than the mean value based on observations (0.48 ± 0.03 °C decade^{-1}). However, similar to winter, the MMM global warming in summer is about 47% stronger than was observed (Fig. 5, Table 1). As a result, the excess European warming relative to the global mean is underestimated by 16% in CMIP6 MMM simulations. The largest contribution to excess European warming in the model simulations is from AER forcing, with an additional smaller contribution from GHG forcing. The responses to NAT forcing are generally weak and make a negligible contribution to the excess European warming.

An additional feature to note in the model simulations is that the sum of MMM European warming trends in response to GHG, AER, and NAT is about 10% weaker in winter and summer than the trends in response to ALL forcings, while the sum of global mean trends is very close to those in response to ALL forcing in both seasons (Fig. 5, Table 1). Three factors may be important for explaining this discrepancy. First, land use and land cover change (included in ALL) might have played a role in local warming over Europe[45,46]. Secondly, there could be nonlinear interactions between the responses to different forcings[47,48]. A third possibility is that the discrepancy may be attributable to internal variability. Understanding these contributions is an important area for future research.

In addition, model simulated warming trends over Europe in response to ALL forcing changes show some spread with a standard deviation of 0.18 °C decade^{-1} in winter and 0.12 °C decade^{-1} in summer among models and a standard deviation of 0.23 °C decade^{-1} and 0.13 °C decade^{-1} in two seasons among different ensembles (Supplementary Fig. S9 and Fig. S10). One important feature to note is that both model spread and ensemble spread of the excess European warming is smaller than the spread of total warming in both winter and summer. This is especially true for the responses to ALL forcings which show 20% - 30% smaller spread in excess European warming than in total warming, suggesting that the excess warming might be a more robust local warming indicator. Understanding both the inter-model spread and the within ensemble spread of responses is an important area for future work.

The contribution of atmospheric circulation to excess European warming in CMIP6 models

We now investigate the contribution of atmospheric circulation to excess European warming in the CMIP6 models. First, we evaluate model simulated interannual variability of SAT and atmospheric circulation over Europe in CMIP6 historical extended all forcing simulations for the period 1979-2020. The standard deviations of circulation indices and European SAT indices show some spread among models and ensemble members but the observed values lie within model range or ensemble range in both seasons (Supplementary Fig. S11). In winter, the MMM SAT interannual variability over Europe is very close to that observed while the MMM NAO interannual variability is slightly lower that the observed value. In summer, interannual variability of European SAT in most models and ensemble members has a similar value to that observed, while interannual variability of the geopotential height index is higher than is observed in some models and ensemble members. The MMM regression patterns of circulation to European SAT in model historical extended simulations in both seasons

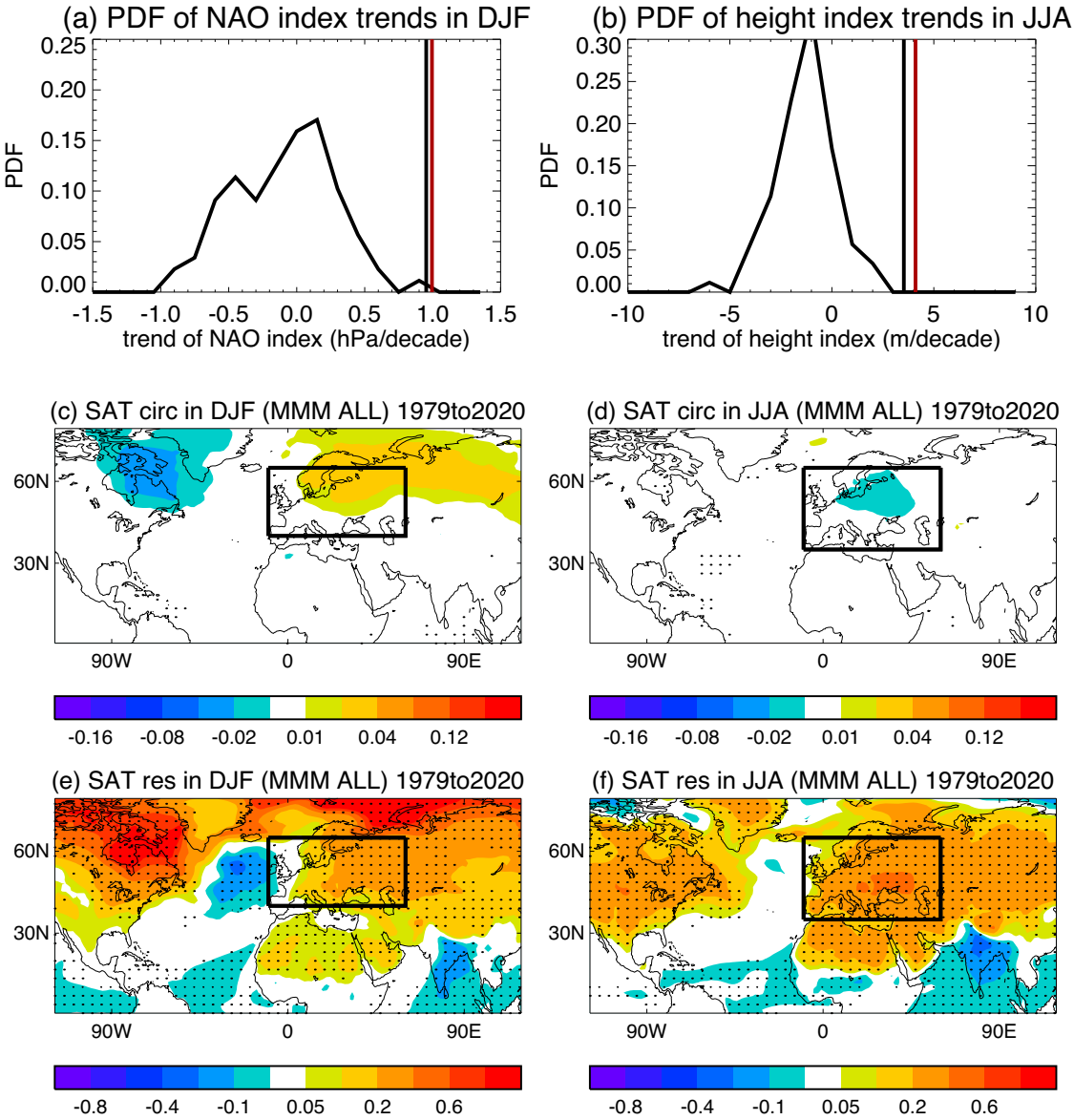

Fig. 6 | Linear trends of atmospheric circulation indices, circulation induced SAT change, and SAT residual in winter (December, January, February) and summer (June, July, August) in reanalyses and CMIP6 historical extended (DAMIP) simulations. a, **b** Probability density function of NAO index trend (hPa decade^{-1}) in DJF and height index trends (m decade^{-1}) in JJA based on CMIP6 historical extended (ALL forcing) ensemble simulations during 1979-2020. Corresponding trends during 1979-2022 based on two reanalysis data sets are plotted as vertical lines (red for ERA5 and black for JRA55). **c**, **d** The multimodel mean (MMM) SAT trend (^{o}C decade^{-1}) due to changes in circulation in DJF and JJA during 1979-2020. **e**, **f** MMM SAT residual trend during in DJF and JJA. The global mean SAT trend is removed in panels (**c**–**f**) and the removal of global mean has a very little impact on panels (**c**-**d**). Note that nonlinear color bar and different colour scales are used in spatial patterns (**c**–**f**). Dots indicate regions where 80% models have the same sign of trend. The black box outlines the region that is used to define SAT index over Europe. The details for analyses of model simulations are in Methods.

show very similar characteristics (Supplementary Fig. S12) in comparison with those based on ERA5 reanalysis (Fig. 2d, e, f, Fig. 3d, e, f). These similar circulation patterns associated with European SAT interannual variability in model simulations and reanalyses indicate a feasibility to investigate the role of atmospheric circulation trends in European warming trends in the CMIP6 model historical simulations. However, there are some regional differences in the MMM regression patterns and those based on ERA5 (Supplementary Fig. S13). The differences show a negative NAO pattern with anomalous easterlies over high latitude and anomalous westerlies over mid-latitude in the North Atlantic in winter, suggesting weaker positive NAO-like circulation associated with warm European SAT variability in multimodel mean simulations than that based on the ERA5 reanalysis. The differences in summer show positive height anomalies over Europe with anomalous easterlies, suggesting stronger height variability associated with warm European SAT in multimodel mean simulations than is found in the ERA5 reanalysis. These regional circulation differences are consistent with Supplementary Fig. S11 which shows NAO interannual variability in most models (ensembles) is underestimated in winter while height interannual variability over Europe in most models (ensembles) is overestimated in summer.

Comparison between the observed trends in circulation indices and the trend distributions derived from the CMIP6 ALL simulations show observed trends in both winter and summer are outside the ranges of those in model simulations (Fig. 6a, b, see Methods). For winter, this result is consistent with the findings of ref. 34. For summer, the result is in line with the findings of ref. 11, who focussed however on heat extremes rather than

mean warming. The MMM circulation trends in winter in ALL simulations project onto the positive NAO phase with increased westerlies downstream of the North Atlantic jet, predominantly due to the response to GHG, but with very weak magnitude (Supplementary Fig. S14a, b, e, f) in comparison with the trends seen in reanalyses (Fig. 2b, c, Supplementary Fig. S2b, c). Circulation responses to AER and NAT forcings are also very weak (Supplementary Fig. S14). The MMM summer geopotential height trends in ALL do not show the observed increase in height over Europe (Supplementary Fig. S15a), but responses to AER forcing show a zonal dipole pattern which has some similarities to the observed trend, albeit with a magnitude about 10% of that based on reanalyses (Supplementary Fig. S15b, Fig. 3c, Supplementary Fig. S4c).

An important consequence of the very weak forced circulation trends seen in the CMIP6 simulations is that the estimated atmospheric circulation contribution to excess European warming is also very small (Fig. 6c, d, Table 2). In winter, atmospheric circulation changes explain 5% ± 10% of the excess European warming (2% ± 4% of the total warming) in CMIP6 simulations, which is less than 40% ± 39% of the excess warming (26% ± 24% of the total warming) estimated from the ERA5 reanalysis. However, the uncertainty in the observed circulation contribution is large owing to large interannual variability and a relatively short record. In summer, atmospheric circulation changes in CMIP6 MMM simulations play a weak damping role for European warming (-4% ± 4% for excess European warming and -2% ± 2% for the total European warming) since the MMM gives a very weak negative geopotential height anomaly over Europe (Fig. 6b, Supplementary Fig. S15a), which is in contrast to the positive contribution to excess European warming (by 29% ± 10%) and total European warming (by 19% ± 6%) estimated from the ERA5 reanalysis. Therefore, *the excess European warming seen in the CMIP6 MMM simulations is almost entirely "thermodynamic" rather than "dynamic", in both winter and summer*. This observation invites us to look again at Fig. 5. Alongside the observed trends, this figure also shows an estimate of the thermodynamic component of observed warming (computed from the residual difference between the actual observed warming and the estimated circulation-related contribution). As the CMIP6 MMM simulations suggest very small circulation-related contribution, it is arguably more appropriate to compare these model results with the observed estimate for the thermodynamic contribution to warming. If we focus on excess European warming (Fig. 5b, d) we see that the trends found in the ALL simulations compare in magnitude well with the estimated thermodynamic contribution in both winter and summer. This suggests that the models may be simulating well this thermodynamic contribution to excess European warming, whilst failing to simulate the dynamic contribution.

Discussion

In this study, we have investigated the causes of "excess" European warming in recent decades, this being a measure of the extent to which Europe has warmed more rapidly than the global mean in both winter and summer. Expressed as a ratio, European temperatures warmed around three times as fast as the global mean temperatures in both seasons. We have shown that this excess warming has both dynamic and thermodynamic contributions. The dynamic contributions are related to trends in atmospheric circulation and, by using a simple regression-based method, we have estimated that these trends can account for about 40% ± 39% (26% ± 24%) and 29% ± 10% (19%% ± 6%) of the excess (total) European warming in winter and summer respectively. These numbers are based on the contribution of a single dominant pattern of atmospheric circulation variability. The uncertainties are larger in winter because the interannual variability is greater. Refs. 11 and[32] reported estimates of the dynamic contribution to trends in summer heat extremes over Western Europe using different approaches. Their estimates of 24% for the trend over 1950-2022[11] and 33% for the trend over 1979-2021[32] are larger than our value of 19% ± 6% for the mean summer warming, but this difference is consistent with evidence that extremes have been warming faster than the mean[11,12,49].

Analyses of CMIP6 MMM simulations show that models reproduce the magnitude of observed European warming quite well. These results suggest that CMIP6 models, unlike previous generations of CMIP3 and CMIP5 models[1,37] do not underestimate European warming in winter and summer; however, they get the right answer for the wrong reasons. As a result, the ratio of European warming to global mean warming in the CMIP6 MMM simulations gives values of 1.8 in winter and 2.1 in summer, which are about 40% and 25% lower than the observed values. The CMIP6 MMM simulations underestimate the magnitude of excess European warming in both winter (by about 43%) and summer (by about 16%), but reproduce the magnitude of thermodynamic excess warming very well in both seasons. However, CMIP6 models do not capture the magnitude of the dynamic warming as a forced response in either season, and the observed circulation trends lie outside the ranges of those in CMIP6 ALL forcing ensemble simulations.

The weakness compared to observations of the regional circulation trends simulated in CMIP6 models has been highlighted in a number of recent studies[11,32,34]. For example, ref. 34 showed that the observed wintertime North Atlantic jet strengthening during 1951-2020 is greater than in any of the 303 simulations from 44 CMIP6 climate models. ref. 32 showed that observed heat extreme trends in summer over Western Europe during 1979-2021 stand out above the 95th percentile of trend distribution simulated by CMIP6 multimodel ensembles. And ref. 11 showed that none of 170 CMIP6 ensemble simulations exhibited a trend in a circulation–induced heat extremes over Western Europe as large as was observed during 1950-2022. These findings are also in line with previous studies which focused on related aspects of European (or wider) climate change[11,18,26,27,32,36,48] and suggest – as also highlighted in these previous studies – either that the circulation response to external forcings is underestimated in the CMIP6 MMM or that low frequency internal variability is underestimated, or both. In either case, these findings imply substantial uncertainty concerning the future rate of European warming, and particularly the dynamical component. However, the situation regarding the thermodynamic contribution to excess European warming looks better. For this component, the CMIP6 MMM agrees well with the observational estimate for both winter and summer. Furthermore, the CMIP6 DAMIP simulations provide quantitative estimates of the contributions from different forcings on European warming in recent decades, identifying GHG forcing as the dominant contribution to the excess warming in winter, but AER emission decline as the dominant contribution to the excess warming in summer. Our findings are consistent with previous studies[18,21] that have highlighted the importance of AER forcing for understanding summer warming in Europe, but also extend these results by quantifying the contributions of different forcings using DAMIP results and by considering excess warming in both winter and summer. These findings have implications for projections. In particular, the large AER contribution to the excess warming in summer is unlikely to be continued in future as it arises from declines in aerosol precursor emissions since the 1970s, which are not expected to continue in future. Thus – if other influences are equal – we should expect excess warming in summer to be lower (perhaps by as much as 60% of the thermodynamic contribution) in future decades than in the recent past. A reduction of the AER contribution would also reduce excess warming in winter, but by a much smaller percentage (up to 15% of the thermodynamic contribution). This study focused on the excess European warming in winter and summer. Previous studies also showed fast surface warming over Europe in spring and autumn[1–3]. Further research to understand the fast warming over Europe in the transition seasons is therefore another important area for future work.

Methods

Reanalysis and observational data sets

The reanalysis datasets used in this study are monthly mean zonal winds on pressure levels, surface air temperature (SAT) and mean sea level pressure (SLP) from the new state-of-the-art climate reanalysis of the European Centre for Medium Range Weather Forecast (ERA5)[50], and the Japanese 55-year Reanalysis Project (JRA55) reanalysis[51] during 1979-2022. The other

observed monthly mean SAT data sets used are the HadCRUT5 dataset[52], the NOAA Merged Land Ocean Global Surface Temperature Analysis (NOAAGlobalTemp)[53], the GISS Surface Temperature Analysis version 4 (GISTEMP v4)[54], and Berkeley Earth Surface Temperatures (BEST)[55]. These reanalysis and observational data sets were interpolated to a common grid with a horizontal resolution of 1.875° longitude by 1.25° latitude. We used monthly mean data to construct boreal winter (December, January, February, DJF) and summer (June, July, August, JJA) means and investigated the trends of surface warming over Europe averaged over the region (45°N-65°N, 10°W-60°E) in winter and over the region (35°N-65°N, 10°W-60°E) in summer. DJF in a year is the mean of December in the previous year, January and February in the current year. We compared these regional warming trends with trends of global means to quantify excess warming over Europe in two seasons. The significance of warming trends at each grid point and the area averaged temperature was tested by the Mann-Kendall nonparametric method. The statistical significance of correlation coefficients between two time series is evaluated based on a two-tailed Student's t-test. The linear trend and the 80% uncertainty range for the regional SAT index for each data set in observations/reanalyses (Tables 1 and 2) were estimated using the ordinary least squares method, taking into account the number of years[56]. The multi-dataset mean warming trend and uncertainty range were estimated from the arithmetic mean of trends and uncertainty ranges based on four observational data sets and ERA5 reanalysis. The uncertainty of warming ratio or circulation contribution to European warming is estimated using the method for the evaluation of standard uncertainty through functional relationships with uncorrelated variables[57]. The uncertainty for variable z = y/x is estimated by the following:

$$(uz/z)^2 = (uy/y)^2 + (ux/x)^2 \quad (1)$$

Where uz is the uncertainty of variable z, uy is the uncertainty of variable y and ux is the uncertainty of variable x.

Estimating the contribution of atmospheric circulation to excess European warming

To quantify the influence of atmospheric circulation change on regional warming trends in observations/reanalyses, we first regressed the detrended atmospheric circulation variables in winter and summer seasons to the detrended surface air temperature index averaged over the region (45°N-65°N, 10°W-60°E) for winter and over the region (35°N-65°N, 10°W-60°E) for summer, where the trends show excess warming compared to the corresponding trends of global means. As discussed in the main text, since the dominant patterns of circulation associated with interannual variability show some similar features to those associated with the multi-decadal (1979-2022) trends in both seasons (Figs. 2 and 3), we next defined a circulation index to quantify the variability in the relevant patterns. For winter, we used an NAO index defined as the difference of area averaged SLP over a southern box (36°N-38°N, 28°W-22°W) around Azores and a northern box (64°N-66°N, 26°W-21°W) around Iceland over the North Atlantic. For summer, we used an index of area averaged geopotential height over the region (40°N-65°N, 5°-50°E) at 500 hPa; in this case we subtracted the trend in the zonally averaged value over the same latitude band to remove the global warming influence on geopotential height. Geopotential height at 500hPa was used to investigate the relationship between large-scale atmospheric circulation, heatwaves, hot extremes and meteorological drought in some previous studies[11,13,32,58]. Studies on hot extremes highlighted the importance of positive feedbacks between soil moisture, atmospheric circulation, and hot temperature, but emphasized that anomalous circulations were initiating these heatwave events and had played a dominant role[59,60].

In a third step, we regressed detrended SAT interannual variations during 1979-2022 onto the detrended circulation indices in winter and summer to obtain spatial patterns of SAT associated with circulation index variability. We then estimated the circulation-related SAT trend by scaling these interannual patterns in proportion to the magnitude of the trend in the appropriate circulation index (Figs. 2g and 3g). The difference between the raw SAT trends and the circulation-related part provides a residual warming pattern (Figs. 2h and 3h), which we interpret over Europe as being primarily related to thermodynamic processes.

In mathematical terms, the regression of detrended SAT onto the detrended circulation index may be expressed as:

$$SAT_{detrended} = a + b \times CI_{detrended} \quad (2)$$

where $SAT_{detrended}$ and $CI_{detrended}$ are detrended surface air temperature and circulation indices respectively, b is the estimated slope and a is the estimated intercept. Then, we rescaled SAT variability using the raw circulation index (CI_{raw}):

$$SAT_{CI} = a + b \times CI_{raw} \quad (3)$$

where SAT_{CI} is total SAT variation (including trend) resulting from circulation variability. The trend in SAT_{CI} is the estimated dynamical contribution to warming at each grid point (Figs. 2g and 3g), and area averaged trends of SAT_{CI} provide estimates of the regional warming trend attributable to changes in circulation.

We repeated our calculations using the ERA5 reanalysis and JRA55 reanalysis and obtained very similar results. We also explored the sensitivity to alternative choices for the circulation indices, namely a zonal wind circulation index at 500 hPa averaged over the North Atlantic jet exit region (45°N-60°N, 50°W-20°E) in winter, and averaged over the Mediterranean (35°N-50°N, 0°-50°E) in summer. As described in the main text, the results were similar to those obtained with our original indices (Supplementary Fig. S3 and S5).

To give context to our results, we also explored an alternative method for estimating circulation related SAT trends over Europe in both winter and summer. We performed empirical orthogonal function (EOF) analysis of circulation variability over the North Atlantic and European sector (25°N-80°N, 60°W-50°E) for SLP in winter, and geopotential height at 500 hPa over the Eastern North Atlantic and European sector (25°N-80°N, 10°W-50°E) in summer using detrended ERA5 reanalysis data. We calculated regression patterns for SAT using each of the principle components. We then calculated the timeseries of circulation indices by projecting original (not detrended) circulation data onto these EOFs, and rescaled regression patterns with each of these timeseries (Eq. 3) to obtain time variations of SAT associated with each EOF. Lastly, we computed the magnitude of the SAT warming trend for Europe associated with each EOF, and also the sum of the contributions to the trend from the leading EOFs. We found that the sums of contributions to European temperature trends from the leading EOFs are consistent with, but slightly smaller than, the trends associated with our index based method. These findings suggest that the circulation indices we use are an efficient way to identify the dynamical contribution to trends in European temperatures.

We note that our method is significantly simpler to some alternative methods[11,32] that have been used in the literature to estimate circulation-related trends. Its simplicity and transparency is an attraction of our method. An additional attraction is that it uses only observational data, with no reliance on climate model data[32]. However, it considers only a single dominant pattern of circulation variability.

CMIP6 and DAMIP simulations

We investigated the impacts of anthropogenic forcings on regional warming trends using multimodel simulations from the Coupled Model Intercomparison Project Phase 6 (CMIP6)[38], including both historical all forcing simulations (referred to as ALL: driven with changes in all anthropogenic and natural forcings) during 1979-2014, extended to 2020 using the SSP2-4.5 future scenario simulations (hereafter as historical extended) and single forcing simulations from the Detection and Attribution Model Intercomparison Project (DAMIP)[39] with the SSP2-4.5 future scenario for 2015-2020. Single forcing experiments include greenhouse gases (GHG) only

(driven with changes in well-mixed greenhouse gas concentrations only), anthropogenic aerosol (AER) only (driven with changes in anthropogenic aerosol emissions), and natural forcing (NAT) only (driven with changes in natural forcings only) simulations during 1979-2020 which were designed to estimate the contributions of different anthropogenic and natural forcings to observed global and regional climate changes. We selected thirteen models that have all the variables needed for all historical and single forcing simulations (Supplementary Table S1). They are the Australian Community Climate and Earth System Simulator Climate Model Version 2 climate model (ACCESS-CM2)[61], the Australian Community Climate and Earth System Simulator Earth System Model version 1.5 (ACCESS-ESM1-5)[62], the Beijing Climate Center Climate System Model (BCC-CSM2-MR)[63], the Canadian Earth System Model version 5 (CanESM5)[64], the National Center for Atmospheric Research Community Earth System Model Version 2 (CESM2)[65], the sixth generation Centre National de Recherches Météorologique Coupled Model (CNRM-CM6-1)[66], the GFDL's Earth System Model Version 4 (GFDL-ESM4)[67], the Goddard Insitute for Space Studies climate model (GISS-E2-1-G)[68], the Hadley Centre Global Environment Model version 3 (HadGEM3-GC31-LL)[69], the Institute Pierre-Simon Laplace Climate Model (IPSL-CM6A-LR)[70], the Model for Interdisciplinary Research on Climate version 6 (MIROC6)[71], the Meteorological Research Institute Earth System Model (MRI-ESM2-0)[72] and the second version of the coupled Norwegian Earth System Model (NorESM2)[73].

We downloaded monthly mean variables from these simulations. Model simulations were interpolated to a common grid with a horizontal resolution of a resolution of 1.875° longitude by 1.25° latitude before the analysis. We used monthly mean data to construct winter (December, January, February) and summer (June, July, August) means and analysed model simulated warming trends over the period 1979-2020 (42 years) in model simulations.

We calculated trends for each member of model experiments with different forcings, performed similar analysis for each ensemble member to separate the role of atmospheric circulation for model simulated warming trend and the residual in CMIP6 historical extended simulations, constructed ensemble mean trends for different forcing experiments for each model, and then constructed the multimodel mean (MMM) by averaging 13 model results (i.e. giving equal weight to each model) for different forcing simulations. The MMM trends in NAT simulations are based on 12 models since some variables in GISS-E2-1-G NAT simulations are not available in the database. The robustness of multimodel simulations was assessed if 80% of models gave the same sign of trends in ALL, GHG, AER, and NAT simulations. To illustrate how unusual of the excess warming over Europe in response to ALL forcing in comparison with warming trend seen in individual ensemble members, we calculated spatial pattern of excess warming in each ensemble member for all models, corresponding inter-ensemble standard deviations in winter and summer and their ratios (signal to noise).

Before we investigated and quantified the role of atmospheric circulations on European warming trends in CMIP6 historical extended simulations, we evaluated model simulated SAT, circulation index variability, and spatial patterns of atmospheric circulation associated with European SAT interannual variability with detrended data to demonstrate that many features of variabilities in SAT and circulation and their associations shown in observations are realistically reproduced by CMIP6 historical ensemble simulations. We calculated circulation index trends for each model and ensemble member for both winter and summer from the CMIP6 historical extended simulations during 1979-2020, and constructed probability density functions for these index trends. Then, we constructed multimodel mean (MMM) warming trends due to changes in atmospheric circulation in CMIP6 historical simulations and MMM residual warming in the same way as we did for the reanalysis data sets and compared model results with the results based on the reanalyses. The 95% confidence interval (CI) for multimodel mean regional warming trends (Tables 1 and 2) were estimated by assuming trends are standard normal distributions and the 95% CI is 1.96 $\sigma/\sqrt{N}$ where σ is standard deviation of regional warming trends among different models and N is the number of models. Therefore, the uncertainty of model simulated regional warming trends is an estimated model structural uncertainty[74]. The uncertainty of warming ratio and in the circulation contribution to European warming is estimated using Eq. (1).

We also estimated contributions of atmospheric circulation to excess European warming based on ERA5 during 1979-2020 and results are very similar to those during 1979-2022 (Table 2). Therefore, trends based on observations/reanalyses were calculated during 1979-2022 and were used in all figures and supplementary figures. Note that trends in observations/reanalyses and model simulations were given by trends per decade to make it easy to compare them except in Supplementary Fig. S1 and S7 where trends during the whole period are given.

Calculating Probability Density Function (PDF) of circulation trends in Fig. 6a, b

We calculated circulation trends for two reanalyses and for each ensemble member of CMIP6 historical extended ALL forcing simulations for all models. We divided the ranges (-1.5 to 1.5 hPa decade^{-1}) for NAO index and ranges (-10.0 to 10.0 m decade^{-1}) for geopotential height index into 20 equal bins and plotted probability of circulation trends in these bins. Figure 6a, b demonstrates that the circulation trends based on two reanalyses are outside the ranges of those based on CMIP6 multimodel ensemble simulations.

Data availability

ERA5 reanalysis is available at https://climate.copernicus.eu/climate-reanalysis. JRA55 reanalysis is available at https://jra.kishou.go.jp/JRA-55/index_en.html and is downloaded from https://rda.ucar.edu/datasets/ds628.1/. HadCRUT5 data set is available at https://www.metoffice.gov.uk/hadobs/hadcrut5/. GISSTEMP v4 is available at at https://data.giss.nasa.gov/gistemp/. NOAAGlobalTemp is available at https://www.ncei.noaa.gov/products/land-based-station/noaa-global-temp. BEST is available at https://berkeleyearth.org/data/. The CMIP6 and DAMIP simulations analysed in this study are versions archived at the Centre for Environmental Data Analysis (CEDA) and they are available at https://help.ceda.ac.uk/article/4801-cmip6-data.

Code availability

All relevant codes used in this work are available, upon request, from the corresponding author B.D.

Received: 3 June 2024; Accepted: 26 November 2024;
Published online: 05 February 2025

References

1. Van Oldenborgh, G. J. et al. Western Europe is warming much faster than expected. *Clim. Past* **5**, 1–12, www.clim-past.net/5/1/2009/ (2009).
2. Twardosz, R., Walanus, A. & Guzik, I. Warming in Europe: Recent trends in annual and seasonal temperatures. *Pure Appl. Geophysics* **178**, 4021–4032 (2021).
3. WMO. *State of the Climate in Europe 2021*. WMO-No.1304, pp52 (2022).
4. Schar, C. et al. The role of increasing temperature variability in European summer heatwaves. *Nature* **427**, 328–332 (2004).
5. Schubert, S. D. et al. Northern Eurasian heat waves and droughts. *J. Clim.* **27**, 3169–3207 (2014).
6. Lorenz, R., Stalhandske, Z. & Fischer, E. M. Detection of a climate change signal in extreme heat, heat stress, and cold in Europe from observations. *Geophys. Res. Lett.* **46**, 8363–8374 (2019).
7. Rousi, E., Selten, F., Rahmstorf, S. & Coumou, D. Changes in North Atlantic atmospheric circulation in a warmer climate favor winter flooding and summer drought over Europe. *J. Clim.* **34**, 2277–2295 (2021).
8. Rousi, E., Kornhuber, K., Beobide-Arsuaga, G., Luo, F. & Coumou, D. Accelerated western European heatwave trends linked to more-persistent double jets over Eurasia. *Nat. Commun.* **13**, 3851 (2022).

9. Bakke, S. J., Ionita, M. & Tallaksen, L. M. Recent European drying and its link to prevailing large-scale atmospheric patterns. *Sci. Rep.* **13**, 21921 (2023).
10. Faranda, D., Messori, G., Jezequel, A., Vrac, M. & Yiou, P. Atmospheric circulation compounds anthropogenic warming and impacts of climate extremes in Europe. *Proc. Natl Acad. Sci.* **120**, e2214525120 (2023).
11. Vautard, R. et al. Heat extremes in Western Europe increasing faster than simulated due to atmospheric circulation trends. *Nat. Commun.* **14**, 6803 (2023).
12. Yin, Z., Dong, B.-W., Wei, W. & Yang, S. Anthropogenic impacts on amplified midlatitude European summer warming and rapid increase of heatwaves in recent decades. *Geophy. Res. Lett.* **51**, e2024GL108982 (2024).
13. Chan, P. W., Catto, J. L. & Collins, M. Heatwave–blocking relation change likely dominates over decrease in blocking frequency under global warming. *NPJ Clim. Atmos. Sci.* **5**, 68 (2022).
14. Christidis, N. & Stott, P. A. Extreme rainfall in the United Kingdom during winter 2013/14: The role of atmospheric circulation and climate change. *Bull. Am. Meteor. Soc.* **96**, S46–S50, https://doi.org/10.1175/BAMS-D-15-00094.1 (2015).
15. Schaller, N. et al. Human influence on climate in the 2014 southern England winter floods and their impacts. *Nat. Clim. Change* **6**, 627–634, https://doi.org/10.1038/nclimate2927 (2016).
16. Blöschl et al. Changing climate both increases and decreases European river floods. *Nature* **573**, 108–111, https://doi.org/10.1038/s41586-019-1495-6 (2019).
17. Philipona, R., Behrens, K. & Ruckstuhl, C. How declining aerosols and rising greenhouse gases forced rapid warming in Europe since the 1980s. *Geophys Res Lett.* **36**, L02806, https://doi.org/10.1029/2008GL036350 (2009).
18. Schumacher, D. L. et al. Exacerbated summer European warming not captured by climate models neglecting long-term aerosol changes. *Commun. Earth Environ.* **5**, 182, https://doi.org/10.1038/s43247-024-01332-8 (2024).
19. Ruckstuhl, C. et al. Aerosol and cloud effects on solar brightening and the recent rapid warming. *Geophys Res Lett.* **35**, L12708, https://doi.org/10.1029/2008GL034228 (2008).
20. Nabat, P., Somot, S., Mallet, M., Sanchez-Lorenzo, A. & Wild, M. Contribution of anthropogenic sulfate aerosols to the changing Euro-Mediterranean climate since 1980. *Geophys. Res. Lett.* **41**, 5605–5611 (2014).
21. Dong, B., Sutton, R. T. & Shaffrey, L. Understanding the rapid summer warming and changes in temperature extremes since the mid-1990s over Western Europe. *Clim. Dyn.* **48**, 1537–1554 (2017).
22. Sjolte, J. et al. Solar and volcanic forcing of North Atlantic climate inferred from a process-based reconstruction. *Climate* **14**, 1179–1194 (2018).
23. Hurrell, J. W. Decadal trends in the North Atlantic oscillation: Regional temperatures and precipitation. *Science* **269**, 676–679 (1995).
24. Delworth, T. et al. The North Atlantic Oscillation as a driver of rapid climate change in the Northern Hemisphere. *Nat. Geosci.* **9**, 509–512 (2016).
25. Iles, C. & Hegerl, G. Role of the North Atlantic Oscillation in decadal temperature trends. *Environ. Res. Lett.* **12**, 114010 (2017).
26. Ballinger, A. P., Schurer, A. P., O'Reilly, C. H. & Hegerl, G. C. The importance of accounting for the North Atlantic Oscillation when applying observational constraints to European climate projections. *Geophys. Res. Lett.* **50**, e2023GL103431, https://doi.org/10.1029/2023GL103431 (2023).
27. Schurer, A. P. et al. Role of multi-decadal variability of the winter North Atlantic Oscillation on Northern Hemisphere climate. *Environ. Res. Lett.* **18**, 044046, https://doi.org/10.1088/1748-9326/acc477 (2023).
28. Sutton, R. & Dong, B. Atlantic Ocean influence on a shift in European climate in the 1990s. *Nat. Geosci.* **5**, 788–792, https://doi.org/10.1038/ngeo1595 (2012).
29. Sutton, R. T. & Hodson, D. L. R. Atlantic Ocean Forcing of North American and European Summer Climate. *Science* **309**, 115–118 (2005).
30. O'Reilly, C. H., Woollings, T. & Zanna, L. The dynamical influence of the Atlantic multidecadal oscillation on continental climate. *J. Clim.* **30**, 7213–7230 (2017).
31. Deser, C., Hurrell, J. W. & Phillips, A. S. The role of the North Atlantic Oscillation in European climate projections. *Clim. Dyn.* **49**, 3141–3157 (2017).
32. Singh, J., Sippel, S. & Fischer, E. M. Circulation dampened heat extremes intensification over the Midwest USA and amplified over Western Europe. *Commun. Earth Environ.* **4**, 432, https://doi.org/10.1038/s43247-023-01096-7 (2023).
33. Chemke, R. & Coumou, D. Human influence on the recent weakening of storm tracks in boreal summer. *npj Clim. Atmos. Sci.* **7**, 86, https://doi.org/10.1038/s41612-024-00640-2 (2024).
34. Blackport, R. & Fyfe, J. C. Climate models fail to capture strengthening wintertime North Atlantic jet and impacts on Europe. *Sci. Adv.* **8**, eabn3112 (2022).
35. Taylor, K. E., Stouffer, R. J. & Meehl, G. A. An overview of CMIP5 and the experiment design. *Bull. Am. meteorological Soc.* **93**, 485–498 (2012).
36. Bhend, J. & Whetton, P. Consistency of simulated and observed regional changes in temperature, sea level pressure and precipitation. *Climatic Change* **118**, 799–810 (2013).
37. Boe, J. et al. Past long-term summer warming over Western Europe in new generation climate models: role of large-scale atmospheric circulation. *Environ. Res. Lett.* **15**, 084038 (2020).
38. Eyring, V. et al. Overview of the coupled model intercomparison project phase 6 (CMIP6) experimental design and organization. *Geosci. Model Dev.* **9**, 1937–1958 (2016).
39. Gillett, N. P. et al. The detection and attribution model intercomparison project (DAMIP v1.0) contribution to CMIP6. *Geosci. Model Dev.* **9**, 3685–3697 (2016).
40. d'Andrea, F. et al. Summer deep depressions increase over the Eastern North Atlantic. *Geophys. Res. Lett.* **51**, e2023GL104435 (2024).
41. Klimont, Z., Smith, S. J. & Cofala, J. The last decade of global anthropogenic sulphur dioxide: 2000–2011 emissions. *Environ. Res. Lett.* **8**, 014003 (2013).
42. Flynn, C. M. & Mauritsen, T. On the climate sensitivity and historical warming evolution in recent coupled model ensembles. *Atmos. Chem. Phys.* **20**, 7829–7842, https://doi.org/10.5194/acp-2019-1175 (2020).
43. Forster, P. et al. Evaluating adjusted forcing and model spread for historical and future scenarios in the CMIP5 generation of climate models. *J. Geophy. Res. Atmos.* **118**, 1139–1150, https://doi.org/10.1002/jgrd.50174 (2013).
44. Smith, C. J. & Forster, P. M. Suppressed late-20th Century warming in CMIP6 models explained by forcing and feedbacks. *Geophy. Res. Lett.* **48**, e2021GL094948, https://doi.org/10.1029/2021GL094948 (2021).
45. Findell, K. L. et al. The impact of anthropogenic land use and land cover change on regional climate extremes. *Nat. Commun.* **8**, 989, https://doi.org/10.1038/s41467-017-01038-w (2017).
46. Winkler, K. et al. Global land use changes are four times greater than previously estimated. *Nat. Commun.* **12**, 2501, https://doi.org/10.1038/s41467-021-22702-2 (2021).
47. Feichter, J., Roeckner, E., Lohmann, U. & Liepert, B. Nonlinear aspects of the climate response to greenhouse gas and aerosol forcing. *J. Clim.* **17**, 2384–2398 (2004).
48. Deng, J., Dai, A. & Xu, H. Nonlinear climate responses to increasing CO2 and anthropogenic aerosols simulated by CESM1. *J. Clim.* **33**, 281–301 (2020).
49. Patterson, M. North-West Europe hottest days are warming twice as fast as mean summer days. *Geophys. Res. Lett.* **50**, e2023GL102757 (2023).

50. Hersbach, H. et al. The ERA5 global reanalysis *Q. J. R. Meteor. Soc.* **146**, 1999–2049 (2020).
51. Kobayashi, S. et al. The JRA-55 reanalysis: general specifications and basic characteristics. *J. Meteorol. Soc. Jpn Ser. II* **93**, 5–48, https://doi.org/10.2151/jmsj.2015-001 (2015).
52. Morice, C. P. et al. An updated assessment of near-surface temperature change from 1850: The HadCRUT5 data set. *J. Geophys. Res.: Atmos.* **126**, e2019JD032361 (2021).
53. Huang, B. et al. Uncertainty estimates for sea surface temperature and land surface air temperature in NOAAGlobalTemp version 5. *J. Clim.* **33**, 1351–1379 (2020).
54. Lenssen, N. J. Improvements in the GISTEMP uncertainty model. *J. Geophys. Res.: Atmos.* **124**, 6307–6326 (2019).
55. Cowtan, K. et al. (Eds). Last modified 2023-08-08 "The Climate Data Guide: Global surface temperatures: BEST: Berkeley Earth Surface Temperatures." Retrieved from https://climatedataguide.ucar.edu/climate-data/global-surface-temperatures-best-berkeley-earth-surface-temperatures on 2024-02-14.
56. Montgomery, D. C. & Runger, G. C. *Applied Statistics and Probability for Engineers 5th edn* (Wiley, 2011).
57. Farrance, I. & Frenkel, R. Uncertainty of measurement: a review of the rules for calculating uncertainty components through functional relationships. *Clin. Biochem. Rev.* **33**, 49 (2012).
58. Kingston, D. G., Stagge, J. H., Tallaksen, L. M. & Hannah, D. M. European-scale drought: understanding connections between atmospheric circulation and meteorological drought indices. *J. Clim.* **28**, 505–516 (2015).
59. Fischer, E. M., Seneviratne, S. I., Vidale, P. L., Lüthi, D. & Schär, C. Soil moisture–atmosphere interactions during the 2003 european summer heat wave. *J. Clim.* **20**, 5081–5099 (2007).
60. Diffenbaugh, N. S. & Ashfaq, M. Intensification of hot extremes in the United States. *Geophys. Res. Lett.* **37**, L15701 (2010).
61. Bi, D. et al. Configuration and spin-up of ACCESS-CM2, the new generation Australian community climate and earth system simulator coupled model. *J. South. Hemisph. Earth Syst. Sci.* **70**, 225–251 (2020).
62. Ziehn, T. et al. The Australian earth system model: ACCESS-ESM1. 5. *J. South. Hemisph. Earth Syst. Sci.* **70**, 193–214 (2020).
63. Wu, T. et al. The Beijing Climate Center Climate System Model (BCC-CSM): the main progress from CMIP5 to CMIP6. *Geosci. Model Dev*. (2019). https://doi.org/10.5194/gmd-12-1573-2019
64. Swart, N. C. et al. The Canadian Earth System Model version 5 (CanESM5.0.3). *Geosci. Model Dev.* **12**, 4823–4873 (2019).
65. Danabasoglu, G. et al. The community earth system model version 2 (CESM2). *J. Adv. Modeli.Earth Syst.* **12**, e2019MS001916 (2020).
66. Voldoire, A. et al. Evaluation of CMIP6 DECK experiments with CNRM-CM6-1. *J. Adv. Model. Earth Syst*. https://doi.org/10.1029/2019MS001683 (2019).
67. Dunne, J. P. et al. The GFDL Earth System Model version 4.1 (GFDL-ESM 4.1): Overall coupled model description and simulation characteristics. *J. Adv. Model. Earth Syst.* **12**, e2019MS002015 (2020).
68. Kelley, M. et al. GISS-E2.1: configurations and climatology. *J. Adv. Model. Earth Syst*. https://doi.org/10.1029/2019MS002025 (2020).
69. Williams, K. D. et al. The Met Office Global Coupled Model 3.0 and 3.1 (GC3.0 and GC3.1) configurations. *J. Adv. Model. Earth Syst*. https://doi.org/10.1002/2017MS001115 (2018).
70. Boucher, O. et al. Presentation and evaluation of the IPSL-CM6A-LR climate model. *J. Adv. Model. Earth Syst*. https://doi.org/10.1029/2019MS002010 (2020).
71. Tatebe, H. et al. Description and basic evaluation of simulated mean state, internal variability, and climate sensitivity in MIROC6. *Geosci. Model Dev*. https://doi.org/10.5194/gmd-12-2727-2019 (2019).
72. Yukimoto, S. et al. The Meteorological Research Institute Earth System Model version 2.0, MRI-ESM2.0: description and basic evaluation of the physical component. *J. Meteorol. Soc. Jpn* **97**, 931–965 (2019).
73. Seland, Ø. et al. Overview of the Norwegian Earth System Model (NorESM2) and key climate response of CMIP6 DECK, historical, and scenario simulations. *Geosci. Model Dev.* **13**, 6165–6200 (2020).
74. Hawkins, E. & Sutton, R. The potential to narrow uncertainty in regional climate predictions. *Bull. Am. Meteorol. Soc.* **90**, 1095–1107 (2009).

Acknowledgements

This work was supported by the Natural Environment Research Council (NERC) Climate Change in the Arctic-North Atlantic Region and Impacts on the UK (CANARI) project (NE/W004981/1) and the Towards an Integrated Capability to Explain and Predict Regional Climate Changes (EXPECT) project by the European Union's Horizon Europe research and innovation programme under grant agreement no.101137656. BD and RS are supported by the UK National Centre for Atmospheric Science, funded by the Natural Environment Research Council. We acknowledge the World Climate Research Programme, which through its Working Group on Coupled Modelling, coordinated and promoted CMIP6. We would like to thank three anonymous reviewers for their constructive comments and suggestions on the early version of this paper.

Author contributions

BD and RS designed research. BD carried out analysis. BD and RS worked together on the interpretation of the results and wrote the paper.

Competing interests

The authors declare no competing interests.

Additional information

Supplementary information The online version contains supplementary material available at https://doi.org/10.1038/s41612-025-00930-3.

Correspondence and requests for materials should be addressed to Buwen Dong.